Antenna Miniaturization using Magnetic Photonic and Degenerate Band Edge Crystals

J. L. Volakis, G. Mumcu, K. Sertel, C.-C. Chen, M. Lee, B. Kramer, D. Psychoudakis and G. Kiziltas
ElectroScience Lab., Electrical and Computer Engineering Dept.
The Ohio State University
1320 Kinnear Rd.
Columbus, OH. 43212

Keywords: Dielectric loaded antennas, ceramics, electrically small Microstrip antennas, frozen mode, unidirectionality, metamaterials, photonic crystal

I. INTRODUCTION

Engineered materials, such as new composites, electromagnetic bandgap, and periodic structures have attracted considerable interest in recent years due to their remarkable and unique electromagnetic behavior. As a result, an extensive literature on the theory and application of artificially modified materials has arisen [1]. Already photonic crystals have been utilized in RF applications such as waveguides, filters, and cavities due to their extraordinary propagation characteristics ([2], [3], [4], [5], [6]). One of the most interesting properties associated with photonic crystals relates to their high Q resonances, achieved when a defect is introduced within the periodic structure. When an antenna element is placed within the high Q cavity, it is then possible to harness the high fields and generate exceptional gain. Experiments have already demonstrated this enhanced gain by placing small radiating elements into a cavity built around a photonic crystal. Specifically, Temelkuran, et.al. and Biswas, et.al. ([7], [8]) reported a received power enhancement by a factor of 180 at the resonant frequency of the cavity. Their specific crystal structure was composed of 15 square cross-section rods (in each plane) having a refractive index of n=3.1. The rod thickness was 0.3cm, with a rod–to–rod spacing of 1.1cm to generate a bandgap between 10.6GHz and 12.7GHz using a total size structure of 16.5cm.

More recently, computations using double-negative materials ([9],[10]) illustrate that extraordinary gain can also be achieved when small dipoles are placed inside other exotic materials that exhibit resonance at specific frequencies. However, a drawback of the double negative and left-handed materials relates to their practical realization. Recently, a new class of photonic crystals was introduced ([11], [12], [13], [14], [15], [16], [17]) from available material structures such as rutile (TiO_2) and CVGs (calcium vanadium garnet). In contrast to the usual PBG structures, these crystals exhibit much larger gain without requiring excessive volume. As such, they may be applicable for hand held devices. Of most importance is also their greater bandwidth and improved matching (due to their resonance away from the band edge). Further, these crystals were shown to exhibit extraordinary antenna gain of 15dB or so when a small dipole is placed within the crystal ([14],[15]).

The goal of this paper is to discuss the potential of these crystals (referred to as magnetic photonic crystals (MPCs) and degenerate band edge (DBE) crystals) for antenna

miniaturization and gain enhancement. Before starting this discussion it is appropriate to make a brief presentation on the unique properties of MPCs and DBE crystals.

A key property of any photonic crystal is to support slow electromagnetic modes associated with a vanishing group velocity $\partial\omega/\partial k = 0$. Ordinary or regular bandgap or bandedge (RBE) photonic crystals display this slow electromagnetic mode as the operational frequency approaches the forbidden propagation bands (band edge operation) (see Fig. 1). Once the wave is inside the crystal, the slow down causes accumulation of

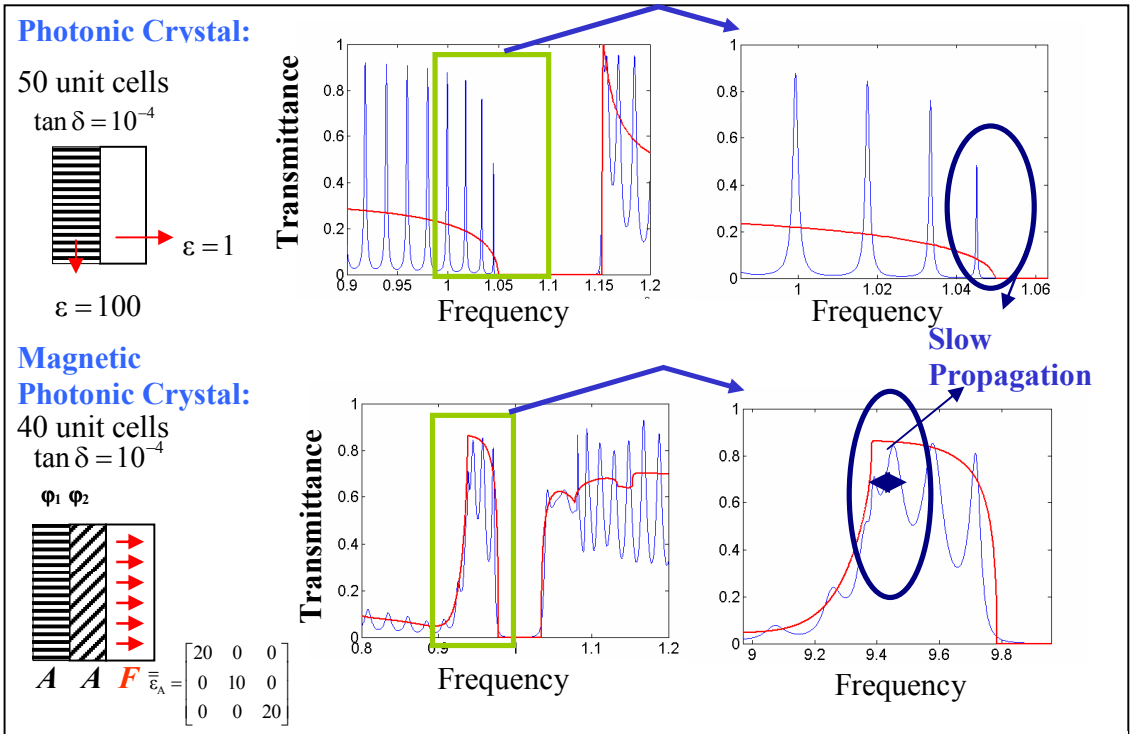

Fig. 1. Transmittance through finite ordinary/regular band edge (RBE) and magnetic photonic crystals (MPC). Note that propagation is at the Fabry–Perot modes (shown as transmittance spikes). Also, note the bandwidth enhancement delivered by the MPCs since several Fabry–Perot modes concentrate to form a continuous transmission band.

the electromagnetic energy (implying higher Q) translating into high radiating power. Therefore, the field amplitude increases much like the case of an enclosed resonator. However, with ordinary photonic crystals, the transmittance vanishes as the operational frequency approaches the band edge (see Fig. 1). Furthermore, the slow down phenomena becomes achievable only at the Fabry–Perot transmittances associated with finite width crystals.

Attention to photonic bandgap (PBGs) materials was first initiated by Yablonovich [18] with the experimental demonstration of modes supported by the well-known wood-pile structure (see also Ho and Soukoulis [19] and Joannopoulos [20]). Some analytical studies of two-dimensional PBG crystals were concurrently carried out by A. Figotin and P. Kuchment ([21], [22]). Research in the RF and Physics community has since then grown substantially, primarily focusing on the experimental investigation of various

periodic dielectric structures (woodpiles, buried dots, cubic lattices, gratings, opals, spirals in silica and dielectric structures embedding periodic metallizations). The recently introduced photonic crystals (see Fig. 1 and Fig. 2) ([11], [12], [13], [14], [15], [16], [17]) alleviate the issue of matching/transmittance and narrow bandwidth. This is done by designing crystals which operate away from the band edge or exhibit a degenerate mode having a much flatter $k-\omega$ response (and therefore a derivative $\partial\omega/\partial k$ which is near zero over a larger band). Specifically, two types of crystals were introduced which concurrently allow for near perfect transmittance (matching) of the incoming wave at the crystal interface. One of the crystals, the MPC, exhibits a stationary inflection point (SIP) in the $k-\omega$ diagram away from the band edge. The other is based on the concept of degenerate band edge. As such, the band diagram of the crystal becomes relatively flat at the band edge as compared to regular band edge crystal. From Fig. 2 it is seen that the DBE for a finite and semi–infinite slab is more matched at the interface experiencing a transmittance rate on the order of $\Delta\omega_d^{1/4}$ vs. $\Delta\omega_d^{1/2}$ for the RBE, where $\Delta\omega_d$ is the difference between the band edge frequency and the frequency of operation. Also, the group velocity decreases more quickly in the DBE ($\Delta\omega_d^{3/4}$) as compared with the

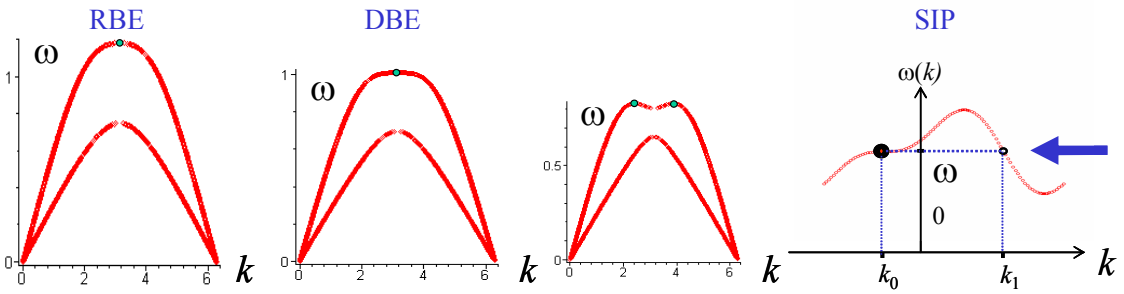

Degeneracy at $\omega=\omega_0$	Group velocity	Saturation Amplitude	Transmittance
2. (RBE)	$(\omega-\omega_0)^{1/2}$	1	$(\omega-\omega_0)^{1/2}$
3. (SIP)	$(\omega-\omega_0)^{2/3}$	$(\omega-\omega_0)^{-1/3}$	1
4. (DBE)	$(\omega-\omega_0)^{3/4}$	$(\omega-\omega_0)^{-1/4}$	$(\omega-\omega_0)^{1/4}$

Fig. 2. Illustration of the band properties of the RBE, DBE and MPC/SIP crystals near there resonance.

$\Delta\omega_d^{1/2}$ rate in an RBE crystal. The consequence of this behavior is a higher amplitude increase in the vicinity of the DBE and MPC based crystals. Equally important is that the DBE and MPC crystals can be smaller than those based on the RBE to achieve the same amplitude increase.

The MPCs include a magnetic layer in their construction. Therefore, although they allow for greater design flexibility and gain, they are more difficult to fabricate and more prone to losses. In contrast, the DBE crystals do not require a magnetic layer in their

construction. Concurrently, they may not reach the better performance associated with the MPC, even though this performance is much improved over that of the RBE (regular bandgap) substrates. Below we present modifications conducted by our group toward miniaturization. These include dielectric loading, impedance matching and antenna termination methods, lumped L/C loading etc. and provide a motivation for using MPC and DBE crystals in antenna design.

II. ANTENNA ENHANCEMENTS USING ORDINARY DIELECTRICS

We recently considered use of ordinary and artificial dielectrics for antenna applications ([23], [24], [25], [26], [27]). We also developed design tools for conformal antenna analysis (see Fig. 3) and proceeded to fabricate samples to validate these antenna designs. The design methodologies were also employed to develop non-periodic textures to enhance

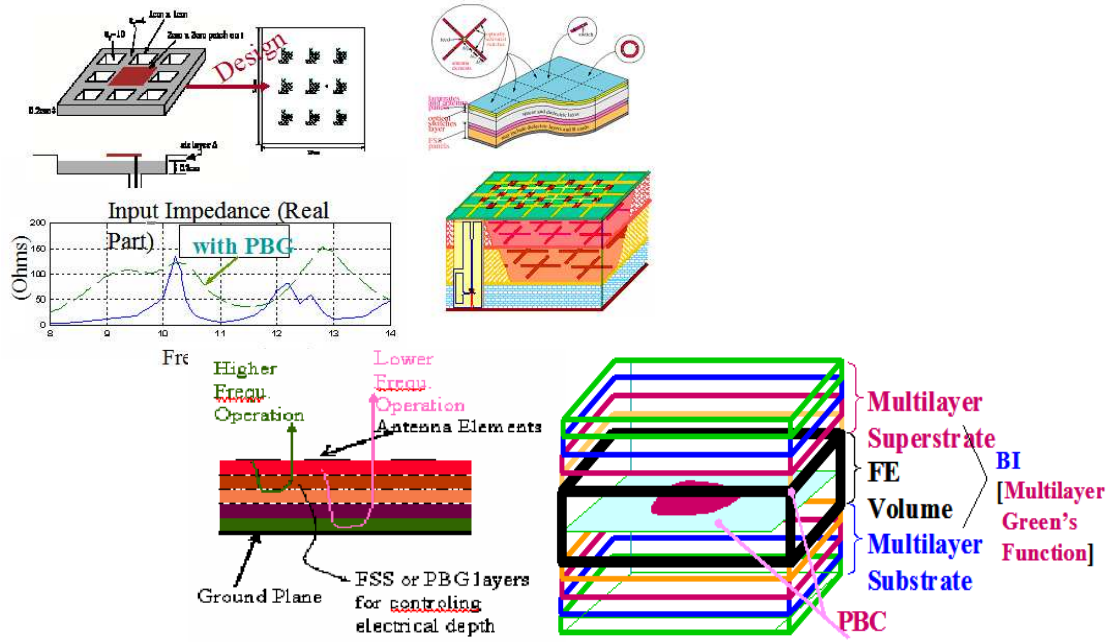

Fig. 3. Antenna and FSS design with periodic substrates to increase antenna bandwidth using our hybrid FE–BI tools shown to the right ([23], [24], [25], [26], [27]).

the bandwidth of traditional narrowband antennas. One of our designs (see Fig. 4) was based on 5 individually textured layers which were fabricated [28] using the method of thermoplastic green machining and measured. The agreement between measurements and calculations is truly remarkable given the "strangeness" of the material design. However, above all, the substantially improved bandwidth (3–fold increase) also demonstrates the potential of material design to improving bandwidth and other classic antenna properties.

A significant part of our most recent work on new materials was focused on antenna miniaturization. We have experimented with both uniform and non–uniform textured designs, and have seen miniaturizations an order of magnitude (factor of 10) without much compromise in performance. As an example, we refer to Fig. 4, where we show square patch printed on a commercial substrate created from a mixture of $\varepsilon_r = 100$ and

stycast having an overall loss tangent of $\tan\delta = 3\times10^{-3}$. The patch planar dimensions are only $\sim 0.1\lambda_0$ (λ_0 = free space wavelength). Even with such a significant miniaturization, the bandwidth is still a remarkable 4.5%. Experience with optimization schemes such as these has shown that they can yield results that are unexpected and not necessarily related to conventional wisdom. It is therefore possible to obtain improved bandwidth or higher gain in a design (for example textured dielectrics), without the mechanism(s) for the improvement(s) being readily understood. In essence, by using a textured dielectric we can pursue more design control. This leads to textured dielectrics (see Fig. 4) that allow for dielectric constant control, important for both impedance matching and bandwidth, when given a set of constraints. An example of a textured substrate is shown in Fig. 5. Here, the textured substrate is truncated to suppress surface wave losses.

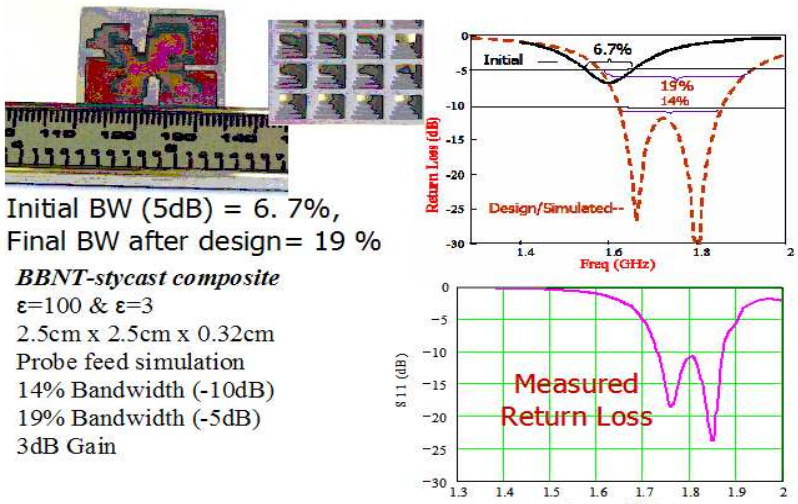

Fig. 4. Designed bandwidth vs. measurements for a simple patch on a multilayered textured substrate. Note the significant improvement in bandwidth.

Also, the feed is placed along the diagonal and the patch's linear dimensions are chosen slightly different to allow for two nearby modes to exist under the patch for increased bandwidth. The resulting patch (with $\varepsilon_{eff} = 23.5 - j0.2$) was found to be 2.5 times smaller than the standard patch on an FR4 substrate. Of importance is that the patch design (see Fig. 5 and 6) exhibits a nearly optimal performance when compared to the Chu limit associated with the Bandwidth – Gain product. This is displayed in Fig. 6 where we compare the performance (see also the associated geometry photos) of our dielectrically modified (metamaterial) antennas. Another optimal antenna [29] (shown in Fig. 7) is a UHF type occupying a 6″ aperture and delivering a gain of 4.5dB with 25% bandwidth. This antenna is ½ the size of and has concurrently 2.5dB more gain than is currently available (to our knowledge). The dielectric loadings in this antenna were mostly used for matching improvements, and occupied a specific (small) region inside the antenna. There was no ground plane used in the simulations and measurements other than the cavity, itself. Were we to employ a ground plane, higher gain could be achieved (geometry details for this antenna and its feeding system can be found in [29]). Clearly, the utilization of materials in antenna design has substantial potential and will likely play a significant role in the future.

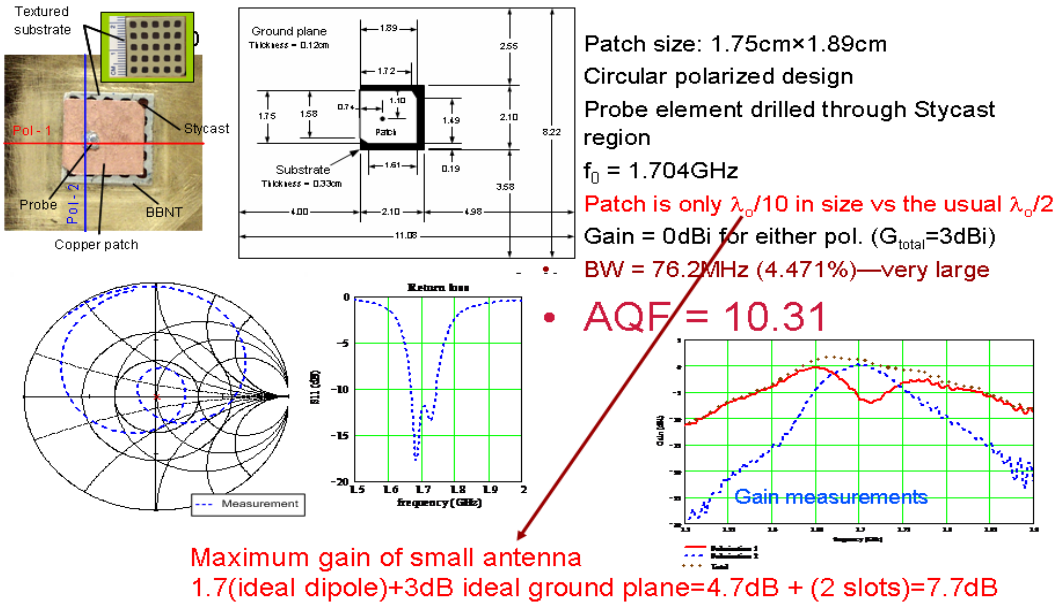

Fig. 5. Geometry of patch design on textured dielectric substrate.

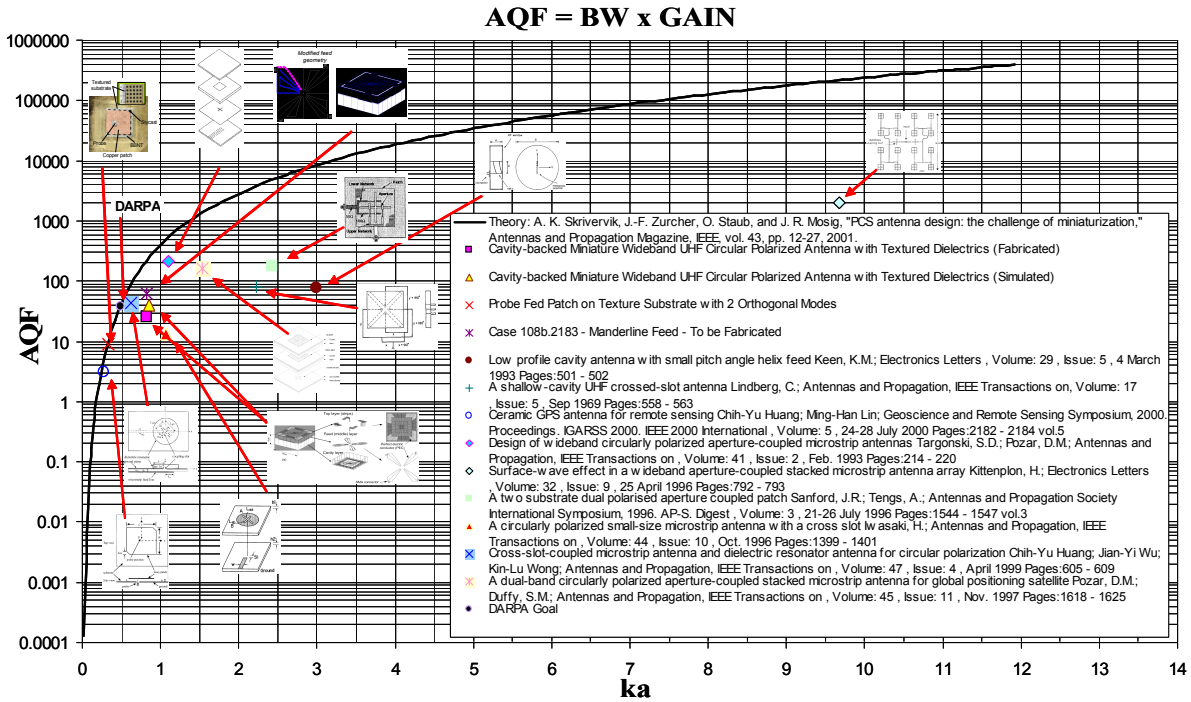

Fig.6. Comparison of the Bandwidth – Gain products for specific antennas designed on textured substrates and for some of the best antennas found in the literature. Note that the black line is the optimal Chu limit. It is important to note that it is more difficult to achieve optimal bandwidth x gain at lower frequencies.

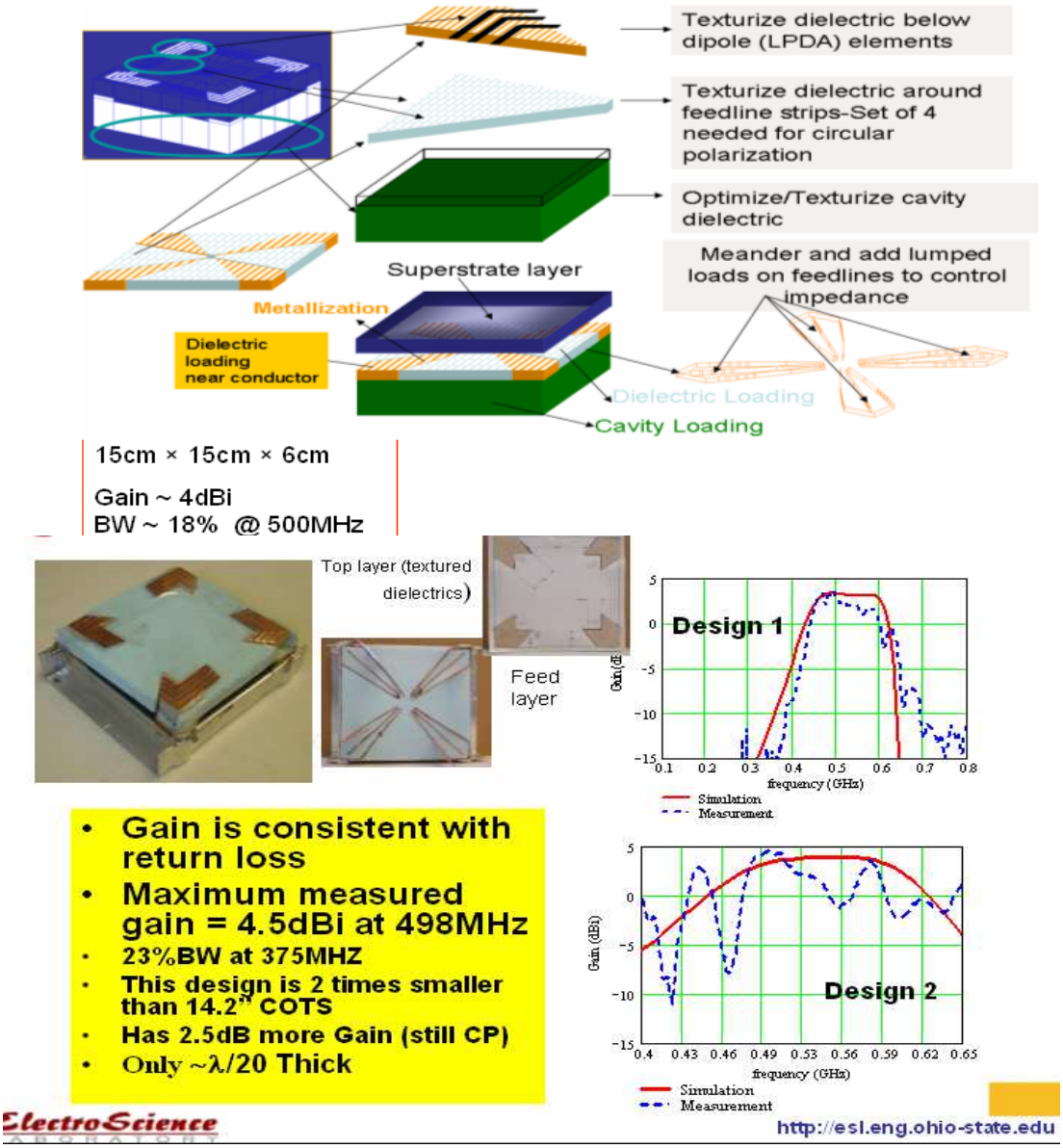

Fig. 7. A metamaterials UHF antenna delivering 4.5dB gain and 23% bandwidth using a $6''$ aperture. Performance is 2.5dB better and size is 2 times smaller than COTS. Note that performance has been verified with measurements.

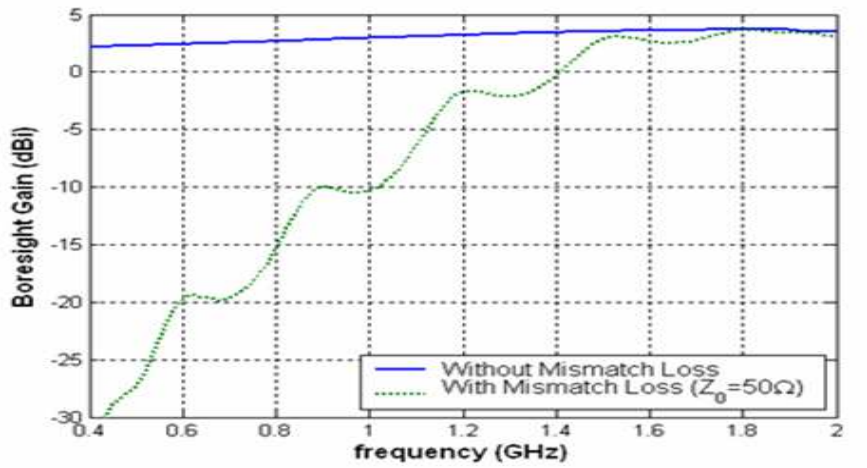

Fig. 8. Improved performance by removing impedance mismatches. It is expected that removal of mismatches will allow for gains of up to 4.7dB even for miniature antennas.

More recently, our focus also turned toward broadband antennas and more specifically to spirals. A challenge in the design of spirals is the ability to maintain good impedance as the frequency is lowered and the aperture becomes only a small fraction (less than 0.1λ). of a wavelength in linear dimensions. Indeed, Fig. 8 shows how impedance matched spirals can deliver the ideal dipole gain with the possibility of even reaching a gain of (for small antennas, less than $\lambda/100$) 5dB when ground plane effects are accounted for. As a further demonstration, we considered how dielectric loading can lead to operations down to a 60MHz (at -10dB gain) using a 10″ aperture and down to 100MHz using a 6″ aperture (see also later in Fig. 10 for similar performance without using magnetic materials). These are truly remarkable miniaturizations, and their realization will be a significant achievement.

The realization of impedance matching with concurrent miniaturization was recently accomplished by introducing artificial lumped loading within the broadband spiral. This concept is displayed in Fig. 9 and relies on individually controlling the L and C loads so that the impedance (Z/Z_0) remains constant with frequency as shown at the top right of Fig. 9. The fact that this impedance matching can be achieved down to low frequencies implies that thin miniature antennas with a diameter as small as 10″ can be allowed to operate down to 100MHz with -15dB gain for a 6″ aperture which scales to 60MHz using a 10″ aperture as illustrated in Fig. 10. These are indeed remarkable performances that could allow the realization of portable antennas that operate down to VHF frequencies.

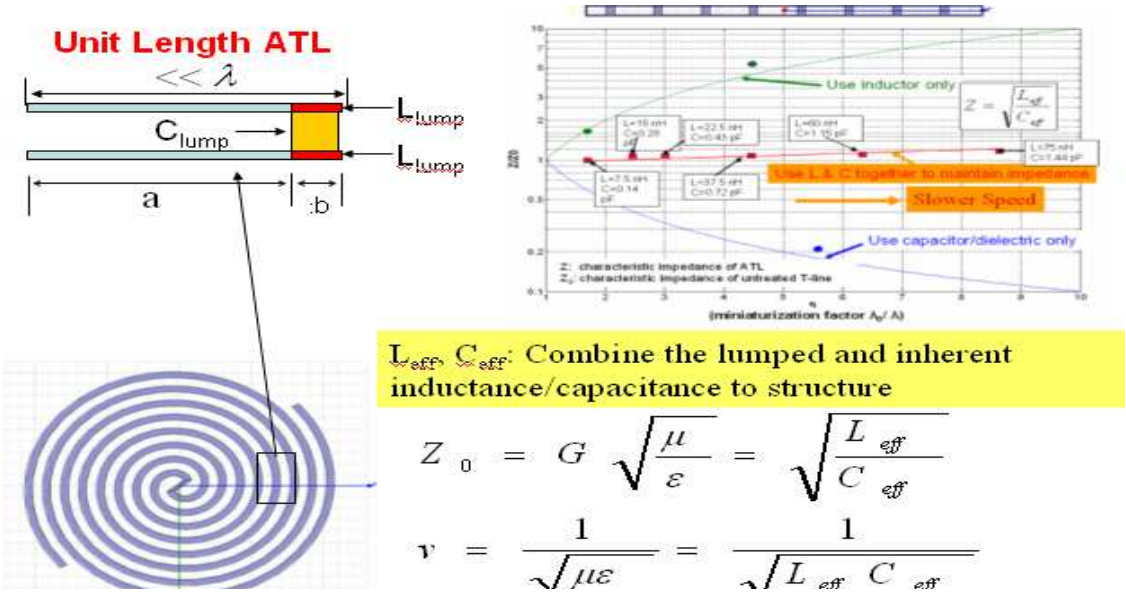

Fig. 9. Illustration of the lumped load concept for concurrent impedance and velocity (miniaturization) control.

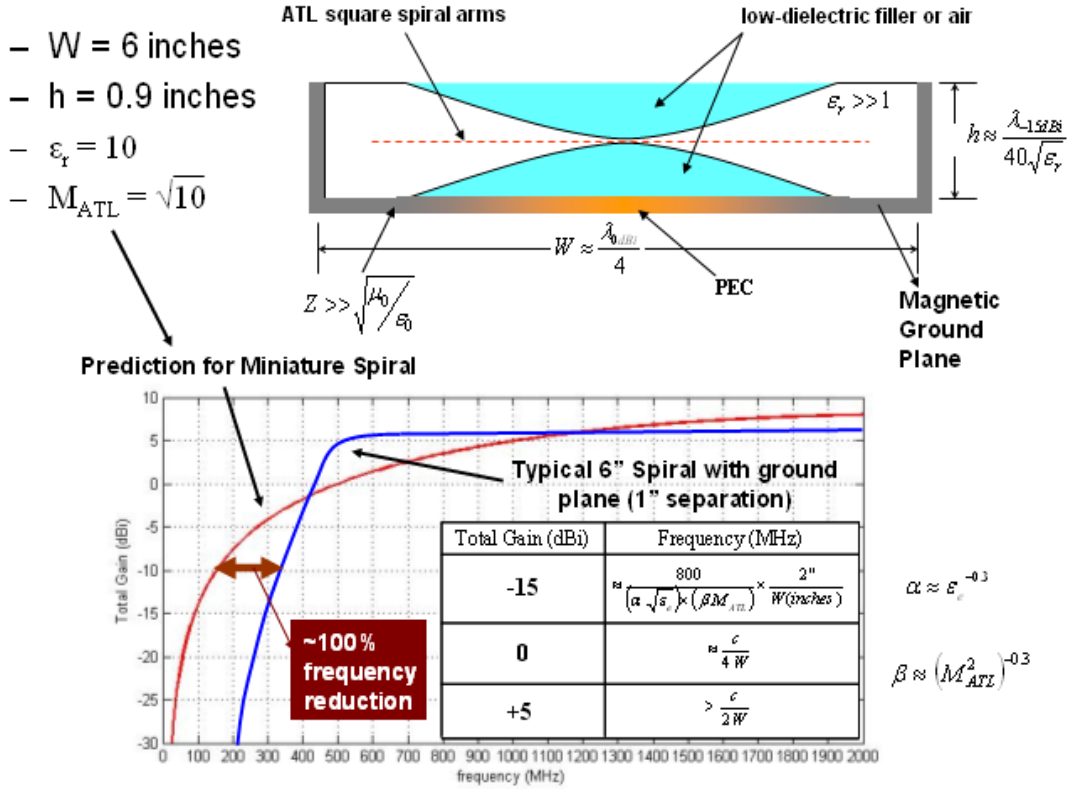

Fig. 10. Miniaturization of a broadband spiral using artificial L/C loading, high contrast ceramic dielectrics, and varying impedance ground plane (from PEC at center to PMC at the edges).

III. PHOTONIC CRYSTALS IN ANTENNA MINIATURIZATION

The benefit of material design for impedance matching and miniaturization was noted above. In fact, Fig. 11 shows even more vividly how material design can significantly improve return loss. Typically, uniform dielectrics are used below the feed lines to obtain a return loss bandwidth of 2% or so for patch antennas. However, by using a tapered dielectric under the feedline (stepped permittivity), the resulting return loss is quite broadband with a bandwidth of at least an octave (over 100%). This is again a demonstration of the potential attributed to material design. As explained below, the recently introduced crystals hold an even greater promise for materials design.

UNIDIRECTIONAL (UD) PHOTONIC CRYSTALS

The recently introduced photonic crystals ([11], [12]) have attractive properties for antenna applications. At RF frequencies, the MPC displays huge effective linear magnetoelectric susceptibility allowing for the realization of electromagnetic unidirectionality (a phenomenon which permits propagation only in one of two opposite directions).

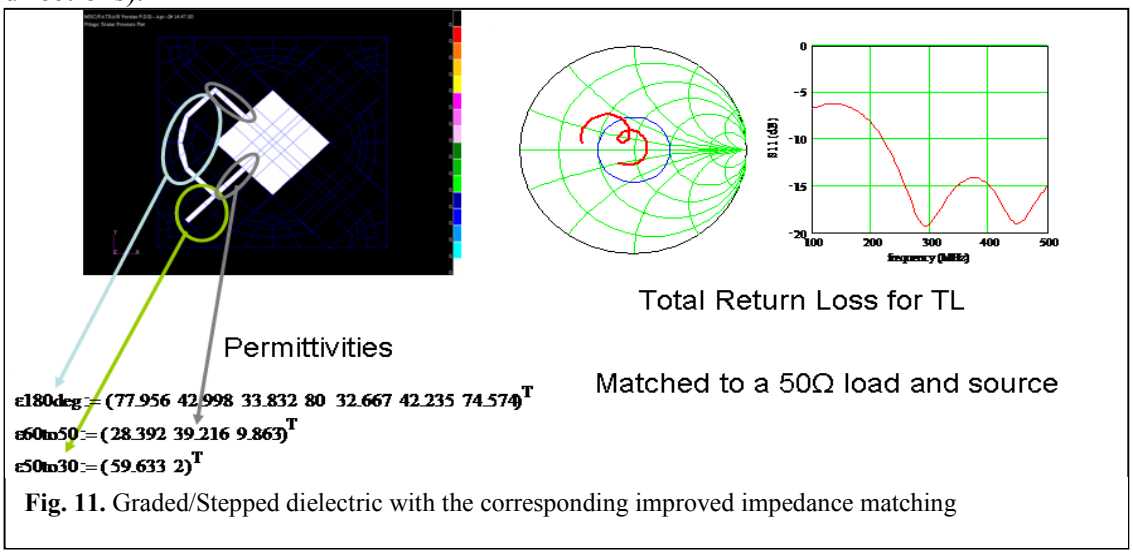

Fig. 11. Graded/Stepped dielectric with the corresponding improved impedance matching

These MPCs (see Figs. 12 and 13) can be considered a generalization of the RBE/PBG crystals discussed above. Their RF behavior is characterized by the bi–anisotropic constitutive relations $\vec{D}=\bar{\bar{\varepsilon}}(\omega)\bullet\vec{E}+\bar{\bar{\alpha}}(\omega)\bullet\vec{H}$, $\vec{B}=\bar{\bar{\mu}}(\omega)\bullet\vec{H}+\bar{\bar{\alpha}}^{T}(\omega)\bullet\vec{E}$, where the linear magnetoelectric effect $\bar{\bar{\alpha}}(\omega)$ is important (but not present in the LH materials or typical PBGs) and is responsible for the unidirectionality and other unique phenomena. Most importantly, the MPCs are based on a combination of available natural materials. Their unique properties for antennas are realized by combining magnetic and dielectric materials, possibly with a bias to introduce Faraday rotation. Magnetic bias also provides for tuning and the potential for broader bandwidth realizations [12].

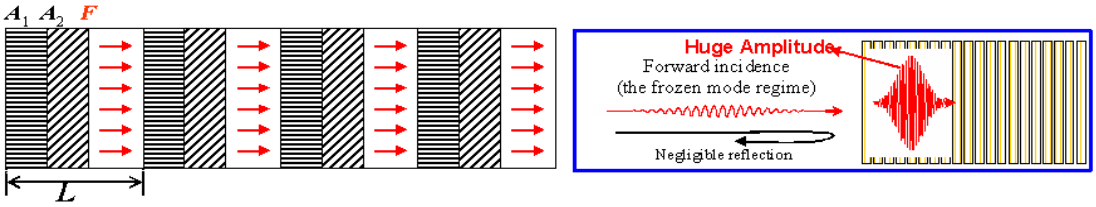

Fig. 12. Illustration of a simplified non-reciprocal periodic stack supporting EM directionality (left) [11]; the right graph illustrates how the incident EM wave on the unidirectional slab gets almost 100% converted into the frozen mode with huge amplitude and nearly zero group velocity.

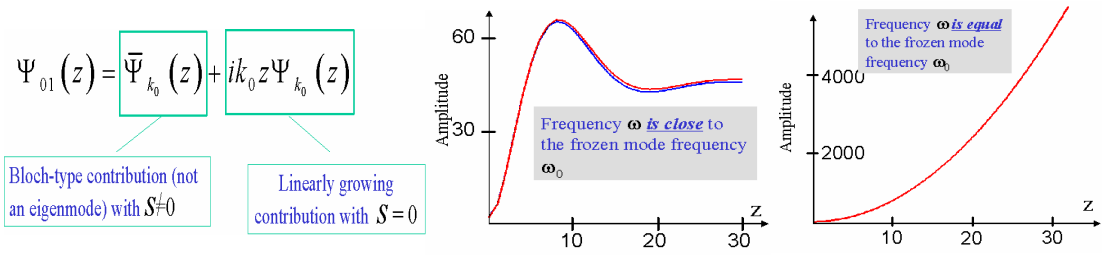

Fig. 13. Relative field intensity W inside the UD slab as a function of distance Z from the vacuum/slab interface. Of interest is the right–most plot where the interior wave grows with Z as it gets converted into the frozen mode [11].

The effect of bulk spectral asymmetry and the electromagnetic unidirectionality requires some minimal degree of complexity of the periodic stack. One of the simplest material combinations (periodic crystal) that can display the unidirectional phenomenon is shown in Fig. 12 (left-most). A unit cell L of this periodic stack is composed of one magnetic and two anisotropic dielectric layers (available commercially). The anisotropy axes of the neighboring dielectric layers must be misaligned with the misalignment angle different from 0 and $\pi/2$. At RF, we can realize the ε layers using textures or embedded inhomogeneities. However, the magnetic layers must be biased with sufficient Faraday rotation (at least 10^0 per λ). Specific matrices for the layers are (ε_D for dielectric layers and ε_F, μ_F for the magnetic layer):

$$\bar{\bar{\varepsilon}}_D = \begin{bmatrix} \varepsilon_D + \delta\cos 2\phi & \delta \sin 2\phi & 0 \\ \delta \sin 2\phi & \varepsilon_D - \delta \cos 2\phi & 0 \\ 0 & 0 & \varepsilon_D' \end{bmatrix}, \quad \bar{\bar{\varepsilon}} \begin{bmatrix} \varepsilon_F & i\alpha & 0 \end{bmatrix} \quad \begin{bmatrix} \mu_F & i\beta & 0 \end{bmatrix}$$

Before proceeding with their use in antenna analysis, we first considered the realization of the frozen mode phenomenon within the MPC. Indeed, it was shown that the frozen mode is realized when $\varepsilon_D = 43.85$, $\delta = 42.64$, and $\Phi = -45^0$ as the misalignment between the dielectric layers. For the magnetic layers, we chose $\varepsilon_F = 30.525$,

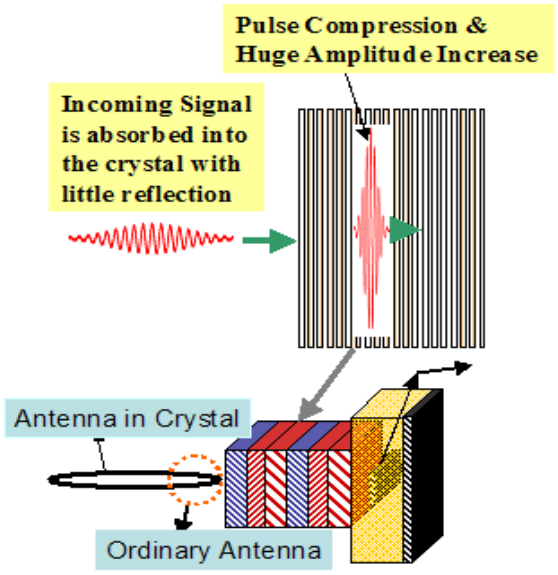

Fig. 14. Illustration of MPC stack design and related benefits

$\alpha = 0.6250$, $\mu = 1.2997$, and $\beta = 1.2432$.

The concept of using MPCs for antenna applications is pictured in Fig. 14. MPCs display several favorable properties for antennas, namely: (a) significant slow down of an incoming wave, resulting in a frozen mode, (b) huge amplitude increase by a factor of 10 to 100, (c) minimal reflection at the free space interface, and (d) large effective dielectric constant, thus enabling considerable miniaturization of the embedded elements [30]. By comparison, ordinary dielectrics cause signal reflection at dielectric interface (mismatches), lowering sensitivity and antenna gain. Thus, small antennas in typical high contrast dielectrics have low sensitivity. As shown in Fig. 15, each MPC unit cell is composed of one gyromagnetic "F" layer (for example, calcium vanadium garnet) and two anisotropic dielectric "A" layers (for example, rutile), misaligned with respect to each other. This type of design and the frozen mode phenomenon have been verified for a finite thickness MPC (consisting of a number of successively placed unit cells) [13]. The main focus is then to harness the resulting high amplitude fields (associated with the

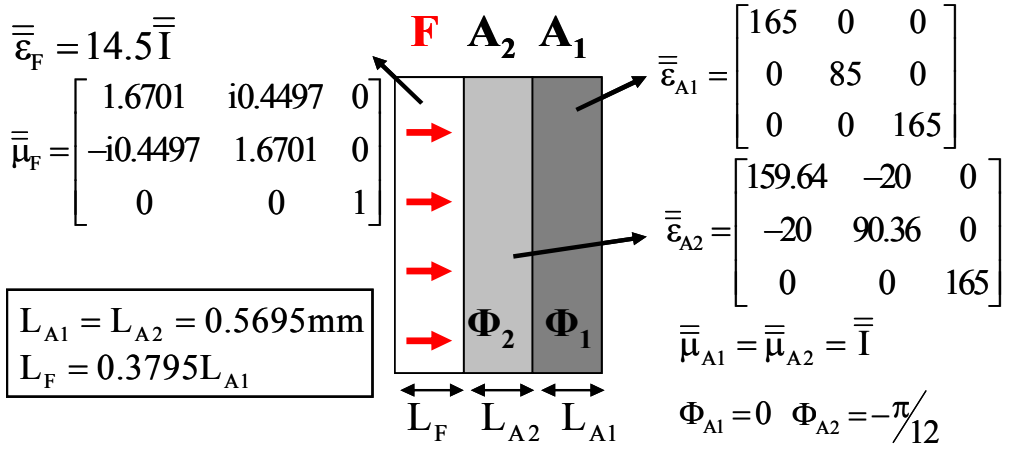

Fig. 15. MPC unit cell. Note the high dielectric, misalignment, and unidirectional property.

frozen mode) and exploit them for electromagnetic applications. This can be done by embedding printed antennas within the MPC structure as discussed below. The large dielectric constant also enables miniaturization of these antennas. Miniaturization then allows for packing very large arrays within a small area to increase power reception/transmission.

COMPUTATIONAL DEMONSTRATION OF A HIGH GAIN MINIATURE ANTENNA

To demonstrate the MPC effectiveness for antenna applications, a computational experiment was conducted as illustrated in Fig. 16. Specifically, a transmitting dipole was placed within the MPC and the moment method technique was used to compute the received power at the dipole terminals due to an incoming wave. Care was undertaken to numerically evaluate the multilayer Green's function for the anisotropic media and in computing the matrix elements for the currents on the dipole. The computational experiment was also extended to arrays embedded within the MPC [30]. The results from these computational experiments were very encouraging. As shown in Fig. 17, the MPC demonstrated that a dipole as small as $\lambda_0/20$ th in size delivers an apparent gain

increase by as much as 15dB higher when placed within the MPC as compared to a dipole in a dielectric of say $\varepsilon_r = 100$. The dielectric slab of $\varepsilon_r = 100$ for comparison was chosen so that the reference antenna element would resonate when its length was also $\lambda_0 / 20$. Furthermore, it was matched to the incoming wave by adjusting the slab thickness to suppress reflections from the slab interface (by $\lambda / 4$ matching). Thus, no penalty was realized due to the dielectric interface mismatches in this comparison (inclusions of such mismatches would be in favor of the MPC). Based on the above explanation, we can conclude that the apparent antenna gain improvement (increase in received power) is purely due to the amplitude growth caused by the MPC when operating at the frozen mode regime. The beam narrowing is actually due to the crystal propagation properties for obliquely incidence waves. This beam narrowing (1/2 power beamwidth was decreased from 45 degrees to 14 degrees) does contribute to added gain, but this gain was not accounted for in the comparisons.

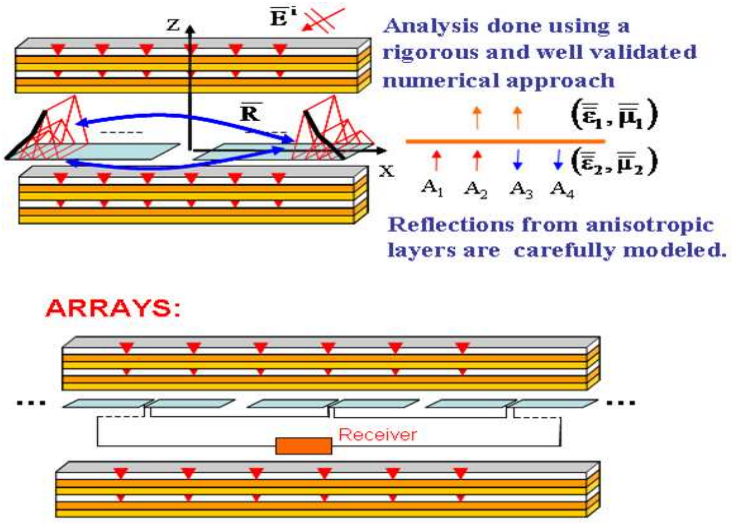

Fig. 16. Illustration of the Computation Experiment to demonstrate high antenna gain.

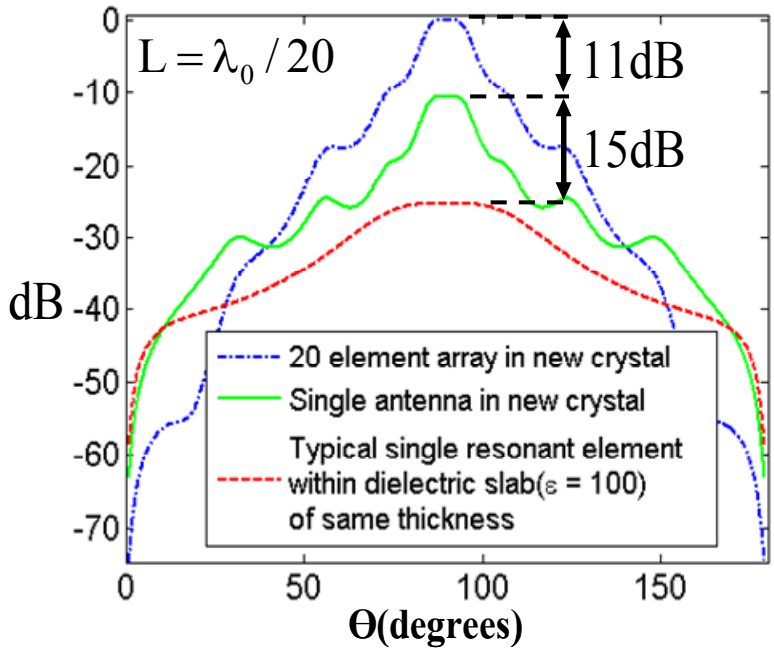

Fig. 17. Results for 2–D miniaturized superdirective antenna array in MPC showing significant gain increase [29].

A 20–element array was also modeled and computed resulting in another 11dB gain for a total of 26dB in more received power.

To summarize, the MPC crystals allow for antennas that are (or have)

- Miniature with extraordinary gain/increased sensitivity (lower power supply requirements)
- 10 times smaller than best available
- High Q with excellent directionality
- 15dB more gain than nominal
- More gain is realized with added array elements (linear increase)
- Reverse biasing for transmit/receive
- Tunable crystal for frequency control
- Natural scanning capability with small frequency modulation

The demonstrated high gain prompts us to proceed with experimental demonstration and verification. Given that the MPCs are unidirectional, a possible transmit/receive configuration can be configured as shown in Fig. 18 using a 5cm x 5cm x 5cm crystal. An added advantage of the MPC is that it generates a narrow beam. This is part of its

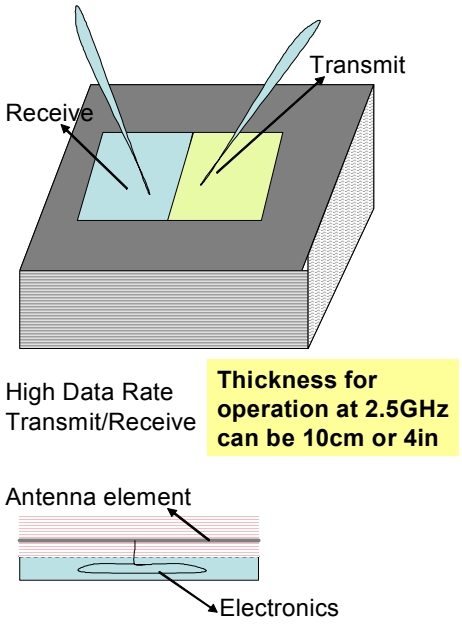

Fig. 18. Concept of operation for the MPC

natural response in the frozen mode regime. More specifically, the frozen mode frequency shifts slightly with the angle of incidence, leading to preferred receptions from only certain angles.

IV. DEGENERATE BAND EDGE CRYSTALS FOR ANTENNA GAIN ENHANCEMENT

As noted above, the MPC crystals require magnetic materials, and are therefore more prone to losses when realized in practice. In contrast, the DBE crystal does not require magnetic layers but still delivers substantial gain increase when the crystals are operated at a Fabry-Perot resonance. Below, we discuss the DBE performance to motivate an optimal design that can be experimentally verified.

As an example, lets us consider a very short strip dipole $\lambda_0/20$ in length (λ_0 is the free space wave length) placed within the crystal that displays degenerate band edge behavior. The width of the dipole is assumed to be 10 times smaller so that it can be considered as a wire dipole. The frequency of operation is chosen to be at the Fabry-Perot peaks discussed earlier (for finite thickness crystals the mode must coincide with the Fabry–Perot peaks). Specifically, the operational frequency is 11.196GHz for N = 20. For this case, the thickness of the crystal is $0.93\lambda_0$ ($0.98''$), but smaller thicknesses can be selected. Since the average dielectric constant inside the crystal is around 100 (as before for the MPC), we compare the performance of the dipole in the crystal with the same antenna embedded within an isotropic homogenous dielectric slab of $\varepsilon_r = 100$. The reference dipole was also of length $\lambda_g/2$, λ_g being the wavelength in the dielectric medium. Further, we chose the thickness of the slab so that it exhibits a $\lambda/4$ matching.

Since, it is much easier to place the dipole antenna at the layer boundaries rather than inside the individual layers, in our analysis, the dipoles were situated on top of the layers that the field attains its maximum value (see Fig. 19). In one case, the dipole was placed within the 10th unit cell at the end of the F layer. The realized gain (increased received power) for this case is shown in Fig. 20 (a), and is seen to be 8.4dB (whereas the MPC gave a gain of about 15dB). We can improve the realized gain by modifying the phase difference (see equations for dielectric tensors) between the layers and by placing the dipole at the end of the A1 layer inside the 11th unit cell. The results of this simulation are given in Fig. 20 (b) and we observe that the realized gain has now been increased to 11.7dB.

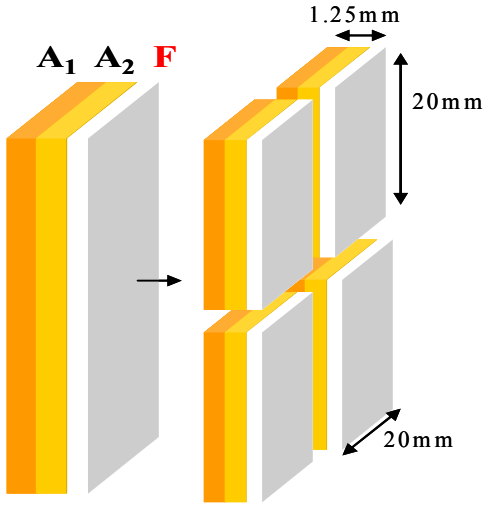

Fig. 19. Structure of the unit cell for the DBE crystals (F layer is air).

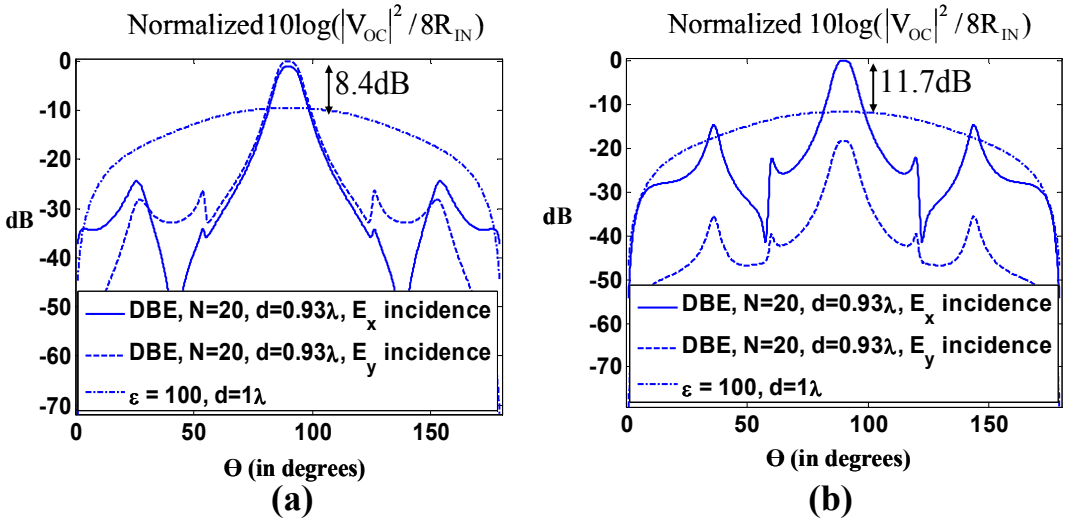

Fig. 20. Radiation of an small dipole inside a DBE crystal (a) Received power for the x and y polarizations with, N = 20, $\Phi_{A1} = 0$, $\Phi_{A2} = \pi/4$ (b) Received power for x and y polarizations in case, N = 20, $\Phi_{A1} = -3\pi/10$, $\Phi_{A2} = -\pi/20$

In Fig. 20 we compare the received power assuming perfectly matched antennas. This is appropriate since the impedances are rather close to each other for different configurations. Specifically, for the reference dipole inside the uniform dielectric, the input impedance is $Z_{DIEL} = 10.85 + j3.5$, whereas in the case of the dipoles inside the DBE crystal, the input impedances are $Z_{CASE1} = 7.31 + j1.8$ (Fig. 20 (a)) and $Z_{CASE2} = 7.2 + j1.4$ (Fig. 20 (b)). It is important to again note that in spite of the high contrast dielectric medium and the smallness of the dipole, the input impedance is quite reasonable. Although the thickness of the crystal is less than λ_0, a significant pattern narrowing (hence directivity improvement) was observed as shown in Fig. 20. Specifically, the half power beamwidth of the dipole is greatly reduced inside the crystal from 76^0 down to 10^0. The same directivity level cannot be achieved using a traditional end fire dipole arrays for the same length. It should also be noted that we have not included this directivity increase in our gain calculations. Our gain calculation only included the increase in the received signal strength and not the directivity. Therefore, this reported gain increase is above and beyond the array directivity increase. We remark that the latter gain enhancement within the MPC and DBE crystals is a direct consequence of the band diagram sensitivity to incidence angle. Since the flatter curve section of the k-ω diagram (associated with the frozen and/or slow modes) occurs at a frequency that depends on incidence angle, the corresponding field amplification is confined to that incidence angle. As seen from Fig. 20 (b) the half power beamwidth is only 8.2^0. The disadvantage of beam narrowing is that scanning is required for reception from all angles. However, this can be an advantage since a simple frequency scanning within a band of 10MHz is sufficient to scan over the entire 180 degrees of space. This is a natural property of the MPCs and DBE crystals. Of paramount importance is that we are able to obtain 11.7dB more gain using a crystal that is only 1″ thick. A high impedance ground plane [31] can only achieve an additional gain of 3dB or so.

Therefore, the potential of these new crystals should provide us with new possibilities in design and realization of miniature, high gain antennas. As an example, these crystals could allow for direct satellite communications using a very small antenna area and low power.

V. CONCLUDING REMARKS

Having demonstrated the potential of MPC and DBE crystals numerically, the next step is their experimental demonstration and verification. A commercially available crystal to be employed in the design is rutile (TiO_2) having $\varepsilon_r = 165$ in the (2^{nd} order isotropic) ab plane and $\varepsilon_r = 85$ in the (perpendicular) c–direction. This crystal was also employed to generate the computational curves in Fig. 20. The rutile samples can be purchased as prisms of dimensions 20–20–2.54mm. For the Fig. 20 simulations, the A layer thicknesses was 0.5mm and the unit cell thickness was 1.25mm. Considering this, we can use 5 layers of rutile from each stack. Since each unit cell requires two rutile layers, we will need about 40 rutile layers to construct the overall crystal.

The intended experiment to be used for demonstrating the crystals is depicted in Fig. 21. The horn antennas at the beginning and end of the structure will be used to excite the crystal and for detecting the transmitted fields at the dipole terminals. With the transmitted field information, our aim is to regenerate the band diagram of the crystal, especially around the degenerate band edge and to realize/measure the best possible gain of the antenna. In addition, we will consider array arrangements and scanning of these to achieve complete spatial coverage. The horn antennas will be, of course, connected to the network analyzer for phase difference measurements. Initially, we will use a monopole antenna implemented by simply removing the cladding at the tip of a coaxial cable. However, other antenna shapes will be used and several computational designs will be considered for improved matching and for array arrangements. The realization of this experiment is currently being pursued.

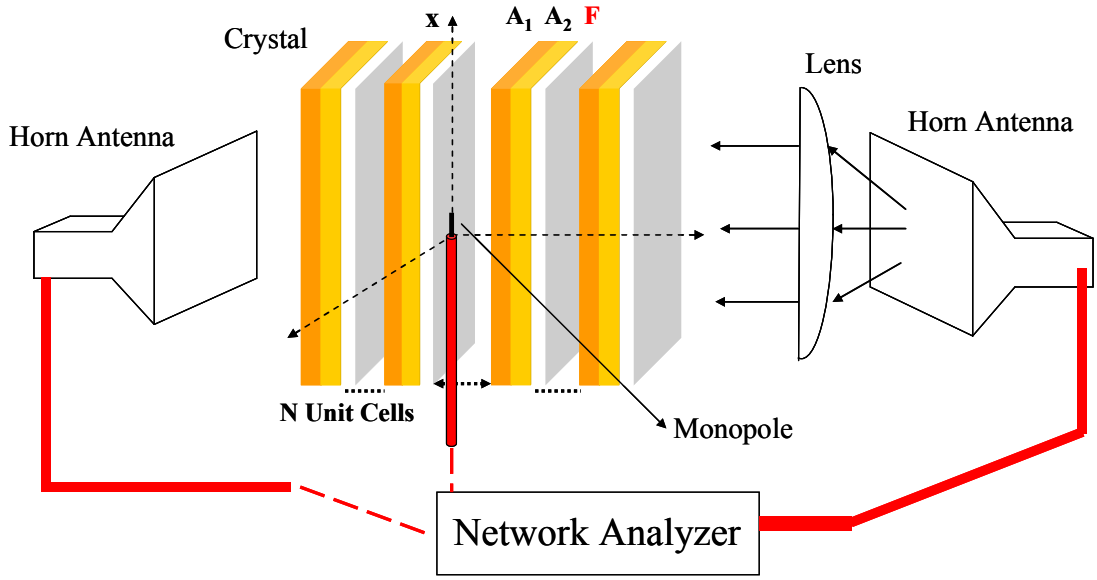

Fig. 21. Experiment setup for measuring the small antenna performance within photonic crystal.

REFERENCES

[1] IEEE Transactions on Antennas and Propagation, Special Issue on Metamaterials, vol. 51, Oct. 2003.

[2] J. Joannopoulos, R. Meade, and J. Winn, Photonic Crystals -Molding the Flow of Light. Princeton: Princeton University Press, 1995.

[3] S.-Y. Lin, E. Chow, V. Hietala, P. R. Villeneuve, and J. D. Joannopoulos, "Experimental demonstration of guiding and bending of electromagnetic waves in a photonic crystal," Science, vol. 282, pp. 274–276, Oct. 1998.

[4] H. Mosallaei and Y. Rahmat-Samii, "Periodic bandgap and effective dielectric materials in electromagnetics: Characterization and applications in nanocavities and waveguides," IEEE Transactions on Antennas and Propagation, vol. 51, no. 3, pp. 549–563, Mar. 2003.

[5] E. Yablonovich, "Photonic band–gap crystals," Journal of Physics: Condensed Matter, vol. 5, no. 16, pp. 2443–2460, Apr. 1993.

[6] D. R. Solli and J. M. Hickmann, "Photonic crystal based polarization control devices," Journal of Physics D: Applied Physics, vol. 37, no. 24, pp. R263–R268, Dec. 2004.

[7] B. Temelkuran, M. Bayindir, E. Ozbay, R. Biswas, M. M. Sigalas, G. Tuttle, and K. M. Ho, "Photonic crystal based resonant antenna with a very high directivity," Journal of Applied Physics, vol. 87, no. 1, pp. 603–605, Jan. 2000.

[8] R. Biswas, E. Ozbay, B. Temelkuran, M. Bayindir, M. M. Sigalas, and K. M. Ho, "Exceptionally directional sources with photonic–bandgap crystals," Journal of the Optical Society of America B, vol. 18, no. 11, pp. 1684–1689, Nov. 2001.

[9] R. W. Ziolkowski and A. D. Kipple, “Application of double negative materials to increase the power radiated by electrically small antennas,” IEEE Transactions on Antennas and Propagation, vol. 51, no. 10, pp. 2626–2640, Oct. 2003.
[10] A. Erentok, P. L. Luljak, and R. W. Ziolkowski, “Characterization of a volumetric metamaterial realization of an artificial magnetic conductor for antenna applications,” IEEE Transactions on Antennas and Propagation, vol. 53, no. 1, pp. 160–172, Jan. 2005.
[11] A. Figotin and I. Vitebsky, “Nonreciprocal magnetic photonic crystals,” Physical Review E, vol. 63, pp. 066 609,1–20, May 2001.
[12] A. Figotin and I. Vitebskiy, “Electromagnetic unidirectionality in magnetic photonic crystals,” Physical Review B, vol. 67, pp. 165 210,1–20, Apr. 2003.
[13] G. Mumcu, K. Sertel, J. L. Volakis, A. Figotin, and I. Vitebsky, “RF propagation in finite thickness nonreciprocal magnetic photonic crystals,” in Antennas and Propagation Society Symposium, 2004. IEEE, vol. 2, Monterey, California, June 2004, pp. 1395–1398.
[14] G. Mumcu, K. Sertel, and J. L. Volakis, “Miniature antennas & arrays embedded within magnetic photonic crystals,” in EPFL Latsis Symposium, Lausanne, Switzerland, Mar. 2005.
[15] J. L. Volakis, C. C. Chen, M. Lee, and B. Kramer, “Miniaturization methods for narrowband and ultrawideband antennas,” in IEEE international workshop on antenna Technology: Small Antennas and Novel Metamaterials, Marina Mandarin, Signapore, Mar. 2005.
[16] A. Figotin and I. Vitebskiy, "Slow light in photonic crystals," arXiv:physics/0504112 v2 19 Apr 2005. (Topical Review, submitted to "Waves in Random and Complex Media").
[17] Electromagnetic unidirectionality and frozen modes in magnetic photonic crystals (Submitted to JMMM)
[18] E. Yablonovich, “Inhibited spontaneous emission in solid-state physics and electronics,” Physical Review Letters, vol. 58, p. 2059, 1987.
[19] K. M. Ho, C. T. Chan, C. M. Soukoulis, R. Biswas, and M. Sigalas, “Photonic band gaps in three dimensions: New layer–by–layer periodic structures,” Solid State Communications, vol. 89, no. 5, pp. 413–416, Feb. 1994.
[20] S. Fan, P. R. Villeneuve, and J. D. Joannopoulos, “Theoritical investigation of fabrication–related disorder on the properties of photonic crystals,” Journal of Applied Physics, vol. 78, no. 3, pp. 1415–1418, Aug. 1995.
[21] A. Figotin and P. Kuchment, Band-Gap Structure of the Spectrum of Periodic Dielectric and Acoustic Media. I. Scalar model, SIAM Journal on Applied Mathematics, 56, No. 1, pp. 68-88, (1996).
[22] A. Figotin and P. Kuchment, Band-Gap Structure of the Spectrum of Periodic Dielectric and Acoustic Media. II. 2D Photonic Crystals, SIAM Journal on Applied Mathematics, 56, No. 6, pp. 1561-1620, (1996).
[23] Z. Li, Y. E. Erdemli, J. L. Volakis, and P. Y. Papalambros, “Design optimization of conformal antennas by integrating stochastic algorithms with the hybrid finite–element method,” IEEE Transactions on Antennas and Propagation, vol. 50, no. 5, pp. 676–684, May 2002.

[24] Y. E. Erdemli, K. Sertel, R. A. Gilbert, D. E. Wright, and J. L. Volakis, "Frequency–selective surfaces to enhance performance of broad–band reconfigurable arrays," IEEE Transactions on Antennas and Propagation, vol. 50, no. 12, pp. 1716–1724, Dec. 2002.

[25] Y. E. Erdemli, R. A. Gilbert, and J. L. Volakis, "A reconfigurable slot aperture design over a broad–band substrate/feed structure," IEEE Transactions on Antennas and Propagation, vol. 52, no. 11, pp. 2860– 2870, Nov. 2004.

[26] G. Kiziltas, D. Psychoudakis, J. L. Volakis, and N. Kikuchi, "Topology design optimization of dielectric substrates for bandwidth improvement of a patch antenna," IEEE Transaction on Antennas and Propagation, vol. 10, pp. 2732–2743, Oct. 2003.

[27] D. Psychoudakis, Y. H. Koh, J. L. Volakis, and J. H. Halloran, "Design method for aperture–coupled microstrip patch antennas on textured dielectric substrates," IEEE Transactions on Antennas and Propagation, vol. 52, no. 10, pp. 2763–2766, Oct. 2004.

[28] A. T. Crumm and J. W. Halloran, "Fabrication of microconfigured multicomponent ceramics," Journal of the American Ceramic Society, vol. 81, no. 4, p. 1053, Apr. 1998.

[29] D. Psychoudakis, J. L. Volakis, Z. N. Wing, S. K. Pillai and J. H. Halloran, "Enhancing UHF Antenna Functionality through Dielectric Inclusions and Texturization", Antennas and Propagation, IEEE Transactions on , vol.54, no.2pp. 317- 329, Feb. 2006.

[30] G. Mumcu, K. Sertel, and J. L. Volakis, "Superdirective miniature antennas embedded within magnetic photonic crystals," in submitted to 2005 IEEE AP-S International Symposium.

[31] R. F. J. Broas, D. F. Sievenpiper, and E. Yablonovitch, "A high-impedance ground plane applied to a cellphone handset geometry," IEEE Transactions on Microwave Theory and Techniques, vol. 49, no. 7, pp. 1262–1265, July 2001.